JOURNAL OF AIRCRAFT
Vol. 38, No. 2, March–April 2001

Using Artificial Neural Networks and Self-Organizing Maps for Detection of Airframe Icing

Matthew D. Johnson* and Kamran Rokhsaz†
Wichita State University, Wichita, Kansas 67260-0044

A method of using artificial neural networks (ANNs) and Kohonen self-organizing maps (SOMs) to detect airframe ice is proposed and investigated. It is hypothesized that ANN systems trained on the aircraft dynamics in real time would converge to different connection weights for iced and clean aircraft. Kohonen SOMs are proposed for detecting these differences automatically and, therefore, recognizing airframe ice accretion. This approach is shown to be capable of acting in an advisory role for the flight crew. The fidelity of the approach is shown to depend on the level of atmospheric turbulence, as well as on the magnitude of the elevator input.

Nomenclature

$[A]$	=	state matrix
$[B]$	=	control matrix
C_{L_1}	=	steady-state trim lift coefficient
C_m	=	pitching moment coefficient
C_x	=	force coefficient along x axis
C_z	=	force coefficient along z axis
$\bar{c}$	=	mean aerodynamic chord
D	=	nondimensional time derivative, $(\bar{c}/2V_c)(\mathrm{d}/\mathrm{d}t)$
i_{yy}	=	nondimensional mass moment of inertia, $8I_{yy}/\bar{c}^3\rho S$
$\bar{q}$	=	nondimensional pitch rate, $q\bar{c}/2V_c$
S	=	wing area
t	=	time
u	=	forward speed perturbation
$\bar{u}$	=	nondimensional perturbation in forward speed, u/V_c
$\{u\}$	=	control input vector
V_c	=	velocity of the center of mass
W	=	aircraft weight
w	=	vertical speed perturbation
$\{x\}$	=	state variable vector
α	=	angle of attack and nondimensional perturbation in vertical speed, w/V_c
δ_e	=	elevator deflection angle
δ_f	=	flap deflection angle
Θ_1	=	steady-state pitch angle
θ	=	perturbation in pitch angle
μ	=	nondimensional mass, $2m/\bar{c}\rho S$
ρ	=	air density
σ	=	turbulence intensity

Introduction

NUMEROUS researchers have investigated the effects of ice accretion on airframe aerodynamics. References 1–6 represent a small cross section of such research. The common conclusion drawn by all of these investigators is that accumulation of airframe ice has very subtle influences on the aerodynamic coefficients, except for the drag, in the linear range of operations. Aerodynamic derivatives, such as the lift-curve slope, are affected minutely by icing. However, large changes in the stall characteristics of airfoils can result from accumulation of ice. Maximum lift coefficients as low as 0.25 have been reported for airfoils such as NACA 23012 (Ref. 6) that otherwise behave well. Such radical departures from normal aerodynamic behavior are generally absent in the linear range. This necessitates the development of methods for clear and correct identification of icing and for alerting the flight crew as to its presence.

Parallel efforts have been underway for many years to understand the effects of airframe icing on the handling characteristics of an aircraft. These efforts have focused on aircraft stability and control characteristics as modified by icing. NASA, using a DHC-6 Twin Otter aircraft, carried out most of the flight tests associated with this research.[7–12] The database generated as a result includes effects of different types and severities of natural and simulated ice.

Ranaudo et al.[10] attempted to quantify the impact of icing on longitudinal stability and control characteristics of the aircraft. They used the modified stepwise regression (MSR) method for parameter identification to determine some of the longitudinal stability and control derivatives of the Twin Otter with and without simulated ice on the horizontal tail. This research was followed by that of Batterson and O'Mara,[11] in whose research the maximum likelihood method was used for such parameter identification. Whereas both of these documents were concerned with the longitudinal stability and control, the lateral–directional case was also addressed in Ref. 12.

In most of the preceding cases, the parameter identification method produced different results for the iced and the clean aircraft. However, the fidelity of the methods seemed to decrease with increasing airspeed, until the results could be called mixed at best. Furthermore, in some of the cases considered, the two different parameter identification schemes predicted different airspeed dependence for some of the stability and control derivatives for the same case.[11] Therefore, none of the methods could be used with certainty to identify airframe icing.

Over the past decade, the study and utilization of artificial neural networks (ANNs) has steadily expanded. These systems are especially suitable for identification and control of highly nonlinear and/or uncertain plants because they do not rely on a detailed knowledge of the plant a priori. One example of such application is that due to Hess[13] where feedforward ANNs were utilized with a backpropagation algorithm to identify the aerodynamic model of a simulated aircraft. This study met with some success, but pointed to the complexity involved in using ANNs to identify and characterize the complete dynamics and aerodynamics of an aircraft. Likewise, Ghosh et al.[14] undertook the task of identifying the lateral–directional stability derivatives using ANN. In this case the authors used a formulation named the delta method to successfully extract the stability derivatives from flight-test data.

All of the preceding parameter identification methods have been successful to one degree or another in estimating aircraft stability and control derivatives. However, they all also lack the fidelity necessary to distinguish clearly and unambiguously the differences

Presented as Paper 2000-4099 at the Atmospheric Flight Mechanics Conference, Denver, CO, 14–17 August 2000; received 24 June 2000; revision received 22 November 2000; accepted for publication 26 November 2000.

*Graduate Research Assistant, Department of Aerospace Engineering. Student Member AIAA.

†Associate Professor, Department of Aerospace Engineering. Associate Fellow AIAA.

between the properties of iced and clean configurations in the linear range of aerodynamic coefficients. The major contributors to this uncertainty are the very subtle changes in the stability derivatives due to icing and the very gradual nature of these changes in the linear range of aerodynamics. McMillen et al.[15] faced a similar problem where the parameters of interest, namely, the fidelity of onboard instrumentation during a flight-test program, changed very slowly over time. After considering a number of models, the authors concluded that in such cases it is best to use a collection of very small networks, each representing one parameter of interest.

The goal of the present research project was to investigate a technique that could identify the presence of airframe ice from the gradual changes in the aircraft dynamics. It was envisioned that such a system could sense such changes and act in an advisory capacity to the flight crew well in advance of the potentially catastrophic consequences of airframe icing. The proposed approach relied on monitoring the aircraft dynamic response to periodic small elevator doublets introduced by the flight control system. This problem had many elements in common with that of Ref. 15. Therefore, the authors believed that a similar approach, coupled with a pattern recognition scheme, could be employed for this purpose. The proposed approach could be used to identify any type of airframe ice accumulation. Nonetheless, due to the availability of flight-test data, this study was limited to the effects of horizontal tail ice only. Also, being a feasibility study, the present work was limited only to investigating the longitudinal modes of motion.

Method of Analysis

Overview

The method of analysis used in this project can be summarized in the following four steps:

1) Periodically, perturb the aircraft with a small doublet elevator input and record the response time history.

2) Use the time history of each state variable to train an ANN dedicated to that state variable.

3) Use the networks' connection weights as input to a self-organizing map for comparison with those obtained at several preceding time steps. Airframe ice accretion will result in differences between the current connection weights and those of the preceding time steps.

4) In the case of longitudinal motion, there will be a set of four votes by the system, one based on each state variable. These votes can act in an advisory role for the flight crew to take appropriate action.

In the absence of an unlimited number of flight-test data sets, the aircraft response was numerically simulated. The fidelity of this simulation was verified through comparison of its results with those from an actual flight test.

Aircraft Geometric Model

The only experimental data available for this study were those used in Ref. 12 pertaining to a DHC-6 Twin Otter. Therefore, without any loss of generality, this aircraft was modeled and used for the present investigation. Table 1 shows some of the pertinent geometric and inertial data for this aircraft.

Table 1 Geometry and inertial properties of the baseline DHC-6 Twin Otter

Property	Units	Value
Inertia:		
Mass	slug	328
I_{yy}	slug · ft^2	25,000
Geometry:		
Wing area	ft^2	420
Wingspan	ft	65
Wing mean chord	ft	6.5
Wing aspect ratio	——	10.0
Horizontal tail area	ft^2	99.1
Horizontal tail span	ft	20.8
Horizontal tail aspect ratio	——	4.35

Table 2 Stability derivatives for the clean DHC-6

Derivative[a]	Estimated[9,10]	Calculated[16,17]
C_{x_u}	——	−0.3
C_{z_u}	——	−0.24
C_{m_u}	——	0
C_{x_α}, rad^{-1}	——	0.43
C_{z_α}, rad^{-1}	−5.6	−5.8
C_{m_α}, rad^{-1}	−1.3	−2.5
$C_{z_{\dot\alpha}}$, rad^{-1}	——	−2.2
$C_{m_{\dot\alpha}}$, rad^{-1}	——	−7.9
C_{z_q}, rad^{-1}	−25	−6.6
C_{m_q}, rad^{-1}	−38	−27
$C_{L_{\delta e}}$, rad^{-1}	0.9	0.76
$C_{m_{\delta e}}$, rad^{-1}	−2.0	−2.57

[a]Subscripts denote derivatives, unless stated otherwise.

Aircraft Dynamic Model

Longitudinal equations of motion were used to simulate aircraft response to doublet elevator inputs. Because the method concerned flight in the linear range of aerodynamics, linearized equations of motion were used for dynamic modeling as well. These equations, in nondimensional state variable form, can be summarized as

$$\{\dot{x}\} = [A]\{x\} + [B]\{u\} \tag{1}$$

where

$$\{x\} = [\bar{u}, \alpha, \theta, \bar{q}]^T \tag{2}$$

and

$$\{u\} = [0, 0, 0, \delta_e]^T \tag{3}$$

The elements of the state matrix $[A]$ and the control matrix $[B]$ are given in the Appendix. The notation used here is consistent with that of Ref. 16.

The stability derivatives present in these equations were estimated using a combination of methods from Etkin[16] and Roskam.[17] The details of estimating these derivatives are given in Ref. 18. These quantities, given in Table 2, were checked against those obtained from parameter estimation for the same aircraft. In most cases, the two sets of numbers agreed rather well. However, where the two did not agree, the numbers that appeared more reasonable were employed in the equations.

The effects of tail ice were simulated by varying those derivatives that depended directly on the aerodynamic characteristics of the tail, namely, the lift-curve slope and the drag coefficient of the tail. Because the available flight-test data were from artificial tail ice, no inertial corrections were made to the aircraft model to simulate the presence of ice. Equations of motion were solved numerically using the Euler method with sufficiently small time steps to ensure convergence. The level of agreement between simulation and flight-test data is shown in Fig. 1. In this case, the experimental data were obtained with artificial moderate glaze ice on the horizontal tail and with retracted flaps. The two sets of simulated data shown here were generated with control derivatives calculated from the methods of Refs. 16 and 17 and with control derivatives obtained from parameter estimation.[12] As indicated here, the control derivatives obtained by parameter estimation[12] resulted in better agreement between the flight-test data and simulation time histories. Therefore, throughout the project, values of these derivatives obtained from parameter estimation were used whenever possible. Similar agreements between simulation and experimental data were also obtained for the clean configurations.[18]

Solutions of this type were used to train a set of ANNs, one for each of the state variables. After sufficient training, the connection weights of these networks were used as input to self-organizing maps to determine whether the airframe was iced or not. It is essential to realize that, in actual operation, the aircraft model would not be necessary and these data would be provided by onboard instruments in response to periodic perturbations in elevator deflection angle.

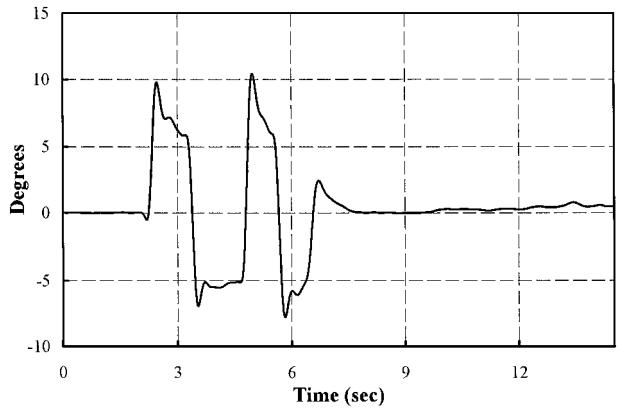

Elevator deflection time history

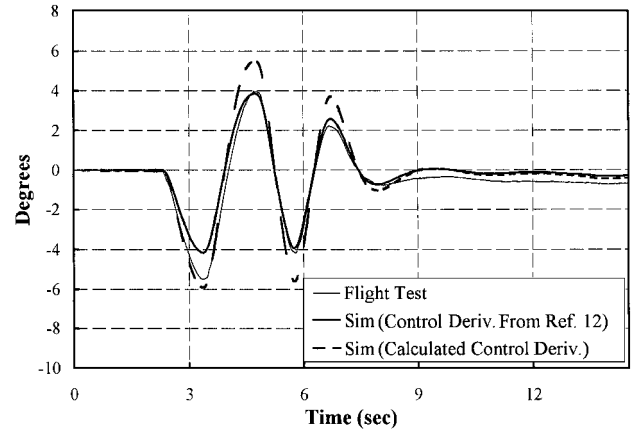

Angle of attack perturbation

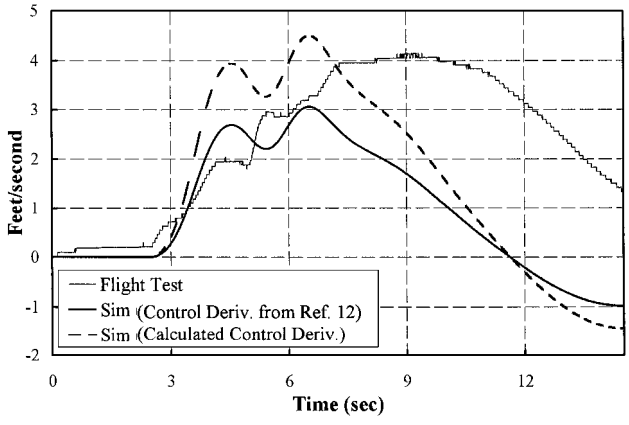

Forward speed perturbation

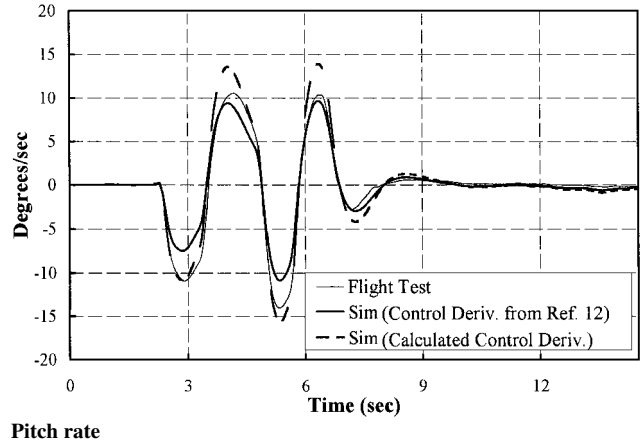

Pitch rate

Fig. 1 Simulated response compared with flight test for moderate glaze ice on the tail and no flap deflection.

Neural Network Models

ANNs have increasingly been shown to be viable tools for mapping nonlinear systems and for the purpose of parameter identification. The basic structure of an ANN is briefly discussed here, before the specific approach used for this research is described. For a more elaborate description, including the details of an ANN's implementation, consult standard texts on the subject.[19–22]

An ANN consists of a collection of neurons arranged in layers. Each neuron receives its signals from a collection of other neurons and passes the sum of the signals, after multiplying it by a nonlinear function (activation function), to the neurons in the next layer through weighted connections. The input and the output layers have one neuron for each input parameter or output parameter, respectively. The layers between these (hidden layers) have as many neurons as the complexity of the data requires, in as many layers as required, but generally fewer than three layers. Each connection between neurons is assigned a weight. These weights are adjusted during training until the ANN learns to associate known sets of input with their corresponding known sets of output (training pairs). In a fully connected ANN, there are also direct weighted connections between the input and output neurons. A diagram of a fully connected ANN is shown in Fig. 2.

Attempts at constructing a single ANN that would predict the future values of all four state variables, given the present and the past values, led to large networks that required long training times, unsuitable for real-time in-flight ice detection. Therefore, each state variable was assigned a small ANN with four input neurons, two neurons in the hidden layer, and one output node. The inputs consisted of the current and past values of the state variable and the elevator deflection angle, and the output was the projected value of the state variable at the next time step. The input and the output neurons used linear activation functions, whereas sigmoid activation function was employed for the hidden layers.

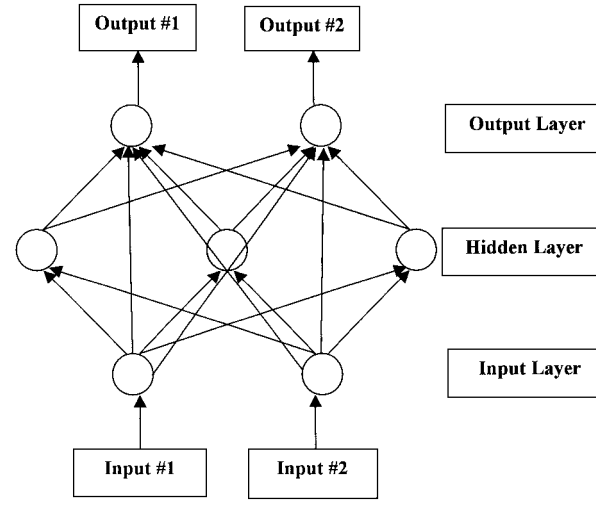

Fig. 2 Schematic of fully connected ANN.

One of the problems associated with an ANN is that two networks starting with two different sets of weights may arrive at two different sets of final weights after training. This is a natural consequence of a nonlinear mapping in which there may be more than one relationship between the input and the output. In the present case, it was envisioned that in actual operation, in the absence of large changes in flight conditions, the connection weights of each network would be used as the starting point to train the same network at the next time period. This strategy would reduce the training time required at each time step and ensure networks with comparable weights. After sufficient training, the connection weights of

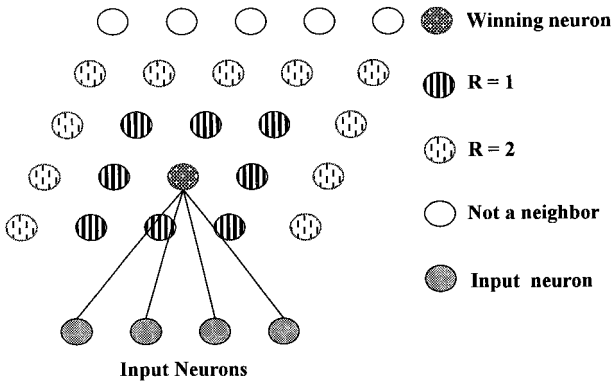

Fig. 3 Architecture of Kohonen SOM.

these ANN models would be used as input to the self-organizing maps, in an effort to distinguish an iced configuration from a clean aircraft.

Self-Organizing Map (SOM)

A self-organizing map (SOM) is a neural network based on competition among neurons. It can be used as a pattern recognition system to order multiple input vectors according to their degrees of similarity. Such a map is a topology-preserving map, meaning that it associates each input vector with a single neuron and places similar input vectors near each other. The network is competitive in that each neuron competes to be the one that corresponds to the input vector.

In a Kohonen SOM, the neurons are arranged in a two-dimensional grid, as shown in Fig. 3. Each input vector has n elements, which also determines the number of connections to each neuron. Unlike conventional ANNs, the neurons are not connected to each other. Training consists of comparing an input vector with each neuron's weight vector to find the one that most closely matches it, based on the inner product of the two. The weight vector of the winning neuron and some of its neighbors are then changed to bring that of the target neuron closer to the input vector. The degree by which the connection weights are modified from one training cycle to the next depends on the degree of agreement between the two vectors, as well as on the distance between a neuron and its neighbors. The magnitude of the adjustments tapers off with distance from the winning neuron. In this manner, the network clusters similar input vectors near each other on the map, with like groups in close proximity and dissimilar groups farther apart. For a more detailed description of Kohonen SOM and its training consult Ref. 23.

In the present research, a one-dimensional SOM was dedicated to each of the state variables. The connection weights of the ANN model of each state variable were used as input to its corresponding SOM. The SOMs were first trained on the data from several earlier time steps and then were presented with the data from the present time. It was reasoned that if the present data belonged to an iced configuration, the connection weights of its state variable ANNs would be different from those of the preceding time steps. Therefore, when presented with both sets of data, the SOM would separate the two and identify the iced configuration. It was understood that because the data from each of the four state variables was processed separately, in certain cases not all four SOM networks would point out icing. In these cases, it was assumed that the crew would resort to a voting system where three out of four indications would be taken as an affirmative vote. The output of such a system is schematically shown in Fig. 4, which points to a high probability of airframe icing. The authors envisioned that this process would be repeated once every 3–5 min onboard an aircraft and that, regardless of the outcome, the newest data would replace the oldest set. The time period of 3–5 min was chosen based on two factors. This period was considered long enough for ice accretion to affect the dynamics of the aircraft without dangerously altering it. Simultaneously, this time period was thought to be short enough not allow significant changes in the inertial properties of the aircraft as the result of burning fuel. In either event, the length of this period would have to be adjusted for optimum ice detection for individual types of aircraft.

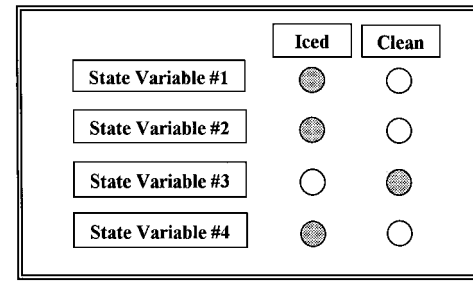

Fig. 4 Schematic of flight crew advisory panel.

Results and Discussion

Flight-Test Data

Flight-test data used for this research were obtained for a DHC-6 Twin Otter aircraft in a comprehensive program on airframe icing at NASA John H. Glenn Research Center at Lewis Field. The specific data used here contained information about 48 sets of tests, flown between December 1991 and June 1992. These flights included 12 sets with the clean aircraft, 8 sets each with artificial ice on the horizontal or vertical tail only, 14 sets with artificial ice on both stabilizers, and, finally, 6 sets with natural ice on the wings. The artificial ice shapes varied from surface roughness to simulate initial stages of icing to moderate rime and glaze ice shapes.

Because the current research concentrated on the longitudinal motion only, the only cases used were those involving elevator inputs. Most of the longitudinal maneuvers were in response to a pair of elevator doublets.

Aircraft Simulation

To assess the effectiveness of the proposed method, the authors needed the time history of the aircraft response to the same elevator input, with and without airframe ice. Flight-test data, although extensive, naturally did not contain data on the exact same configuration flown through exactly the same maneuver, with and without artificial tail ice. Therefore, simulation was used to generate the necessary response time histories. The flight-test data were used for validating these simulations for the clean aircraft and for the aircraft with moderate glaze ice on the horizontal tail. These simulations proved very successful, as shown in Fig. 1, especially when control derivatives obtained from parameter estimation were utilized.

One of the concerns in this approach was the aircraft response to atmospheric turbulence relative to that due to elevator input. Specifically, the authors wanted to know what turbulence level would drown out the effects of ice on the aircraft response. Therefore, the simulation included the von Kármán atmospheric turbulence model given by Hoblit.[24] This model relies on two power spectral density functions, one for vertical and a second one for horizontal gusts. The gust intensity in the simulations was varied from 0.5 ft/s for clear air to 4.0 ft/s for severe storms.[25] Also, the authors made sure that no two simulations were performed with the same turbulence time history, even when all other flight conditions were the same.

Figure 5 shows the relative effects of atmospheric turbulence and simulated tail ice on the response of the aircraft. For these results, the elevator time history was taken from one of the flight tests whose flight conditions are shown in Table 3. Figure 5 shows clearly how tail ice caused measurable changes in the dynamic response of the aircraft. Furthermore, the effect of ice on the response far exceeded that of atmospheric turbulence. The authors aimed to investigate whether these changes could be detected in flight using the proposed approach.

The results shown in Fig. 5 were obtained with an elevator doublet of rather large amplitude. It was reasonable to believe that using such large elevator deflections every 3–5 min would be

Table 3 Flight conditions for flight 181032A, clean aircraft

Property	Units	Value
Airspeed	KIAS[a]	94
Altitude	ft	8064
Temperature	°F	−19
Location of c.g. (from nose)	in.	204.2
Mass	slug	317.7
Flap deflection angle	deg	0

[a]Knots indicated air speed.

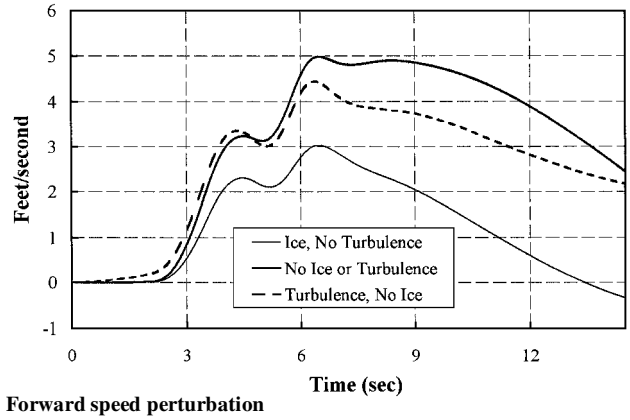

Forward speed perturbation

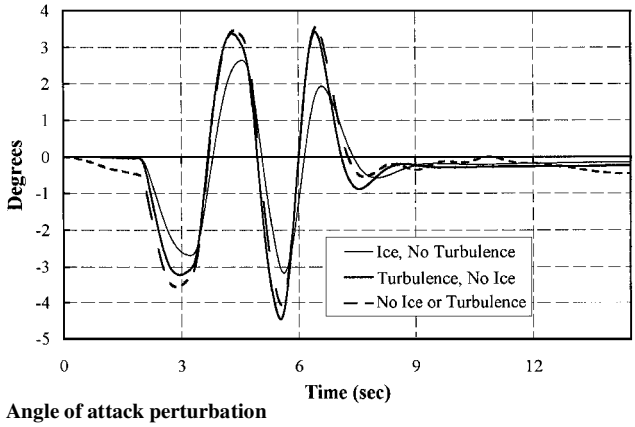

Angle of attack perturbation

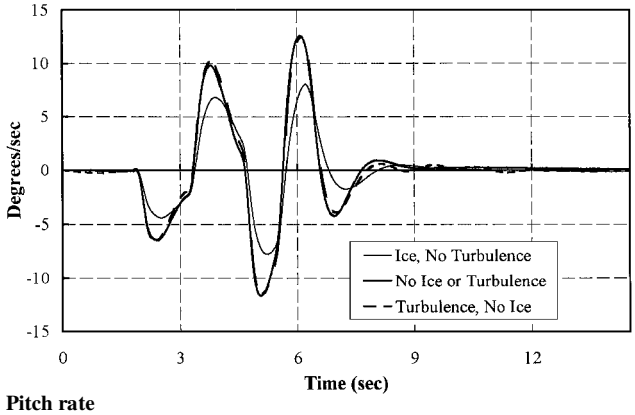

Pitch rate

Fig. 5 Relative effects of simulated tail ice and atmospheric turbulence, σ = 2 ft/s.

unacceptable from the viewpoint of passenger comfort and structural fatigue. On the other hand, as the amplitude of the elevator doublet was reduced, the effects of airframe ice on the response became closer to that of atmospheric turbulence. Therefore, normal acceleration was used to determine the appropriate elevator deflection angle. It was reasoned that an elevator deflection time history resulting in accelerations comparable with those of atmospheric turbulence would be acceptable from the viewpoint of passenger comfort. Furthermore, a smooth curve that would be more reasonable for the flight control system to generate was chosen for the time history of the elevator deflection angle. The new elevator time history and its associated normal acceleration are shown in Fig. 6 along with the normal acceleration generated in cumulus clouds. Based on this and similar simulations, a test matrix of $\delta_{e(\max)} = 0$, 0.025, 0.05, and 0.10 rad was chosen to test the effectiveness of the ice detection system against several levels of turbulence.

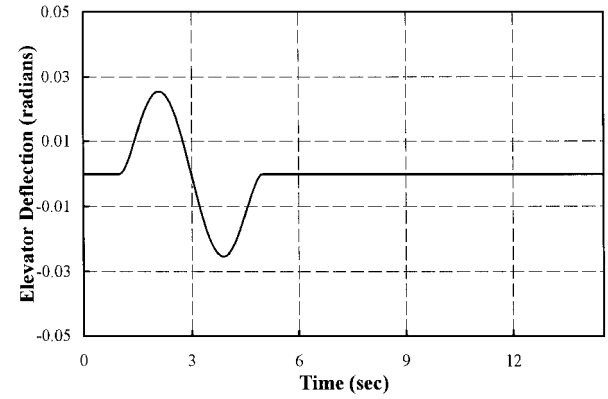

Elevator deflection time history

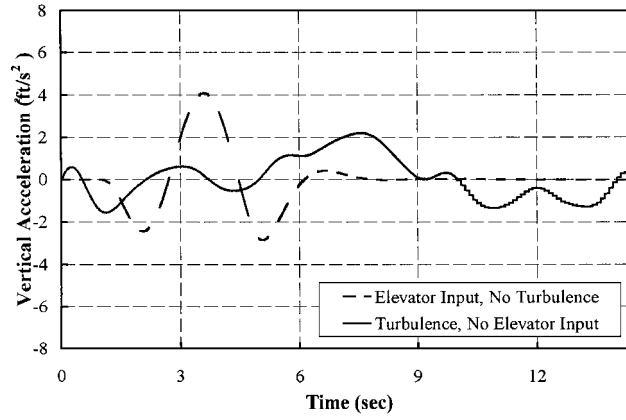

Normal acceleration

Fig. 6 Effect of elevator input compared with turbulence, σ = 2 ft/s.

Neural Network Training

To verify the fidelity of the four ANN models, three separate but similar flight-test data sets were used for training. The ANN models were then tested on a fourth similar data set to see how well they could predict the new set of flight-test data. This procedure was repeated four times, twice with flight-test data of the clean aircraft and twice with flight-test data created with artificial ice on the tail.

The data available for each training set were composed of a possible 1450 data pairs, each pair consisting of the present and the past values of a state variable, the elevator angle for input, and the next value of the state variable for output. Only that part of the data where the response was strongest was used to train the ANNs. This corresponded to a period of 6 s starting with the initial elevator movement. Typical training times on a desktop computer with a 450-MHz processor were 77 s for 20,000 iterations. This number of iterations was necessary for the first cycle that started with a set of random connection weights. Subsequent cycles, each starting with the connection weights of the preceding cycle, required only 7500 iterations each, which were performed in approximately 29 s. In the absence of major changes in flight conditions, such as airspeed or altitude, the first cycle would not have to be repeated. In any case, these times are well below the 3–5 min period that was recommended between every two cycles.

Testing of the ANN models on data that were not used during training produced results similar to those shown in Fig. 7. The flight

Table 4 Flight conditions for flight 210928A, artificial moderate glaze tail ice

Property	Units	Value
Airspeed	KIAS[a]	69
Altitude	ft	5907
Temperature	°F	39
Location of c.g. (from nose)	in.	204.4
Mass	slug	317.0
Flap deflection angle	deg	10

[a]Knots indicated air speed.

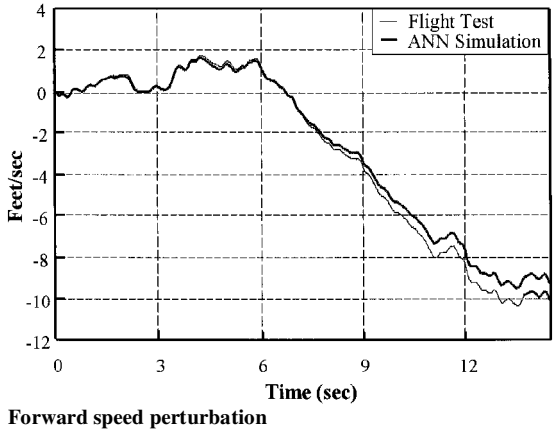

Forward speed perturbation

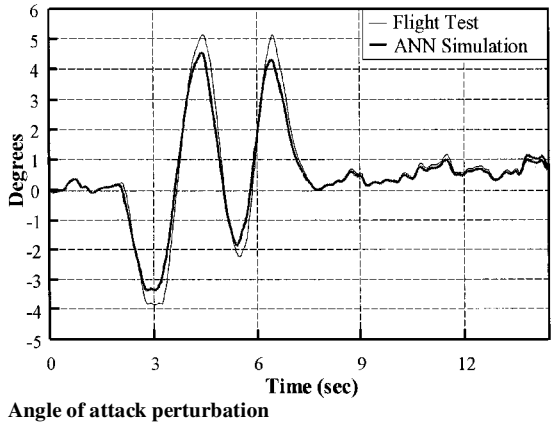

Angle of attack perturbation

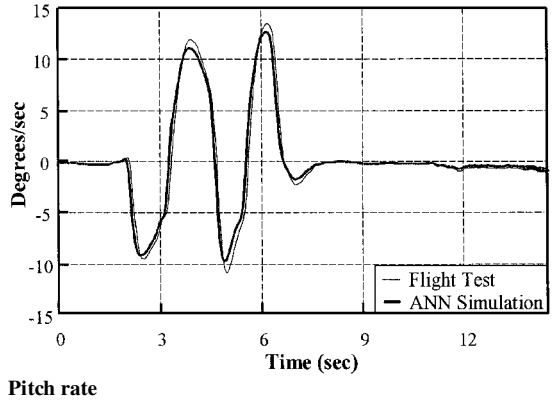

Pitch rate

Fig. 7 Flight-test data compared with ANN model, artificial tail ice, δ_f = 10 deg.

conditions for the flight-test data used here are given in Table 4. The input elevator time history was very similar to that of Fig. 1. These results indicate that the ANN models replicated the flight-test data with remarkable accuracy. Therefore, it was believed that the same accuracy would be achieved when the ANN models were presented with the results generated from simulation for the current research. Again, in actual operation, aircraft instruments would provide the input to the ANN models for training.

Table 5 Parameters varied during simulation

Property	Units	Minimum	Maximum
Airspeed	KIAS[a]	75	100
Altitude	ft	6000	8000
Turbulence intensity σ	ft/s	0	4
$\delta_{e(\max)}$	rad	0.025	0.10

[a]Knots indicated air speed.

Table 6 Success rate of ice detection for moderate glaze ice on horizontal tail

Turbulence intensity σ, ft/s	$(\delta_e)_{\max}$ = 0.025 rad		$(\delta_e)_{\max}$ = 0.05 rad		$(\delta_e)_{\max}$ = 0.10 rad	
	Rate	%	Rate	%	Rate	%
0	12/12	100	12/12	100	12/12	100
1	45/60	75	68/72	94	48/48	100
2	5/24	21	41/72	57	42/48	88
4	6/24	25	15/36	42	25/48	52

SOM Results

To generate data for the SOMs, simulations were performed at varying altitudes, flight speeds, turbulence levels, and maximum elevator deflections. Complete permutation of these parameters is shown in Table 5. For each combination of these parameters, anywhere from 12 to 72 cases were generated. Note that in each case an iced model was compared to four clean models created at the same flight conditions, simulating data taken at four previous times. Even for all parameters being the same, these cases were all different owing to the completely random turbulence time history. These data were then presented to the SOMs, whose success rate at correct identification of airframe icing is shown in Table 6.

In the absence of turbulence, the system detected ice perfectly in all cases. Increasing levels of atmospheric turbulence required larger elevator deflections for successful ice detection. In mild turbulence ($\sigma = 1$ ft/s), the success rate varied from 75 to 100% with maximum elevator deflections ranging from 0.025 to 0.10 rad. However, increasing levels of turbulence intensity reduced the success rate of the system. For $\sigma = 2$ ft/s corresponding to flight in cumulus clouds, the smallest elevator deflection considered here proved insufficient for ice detection, whereas the intermediate value resulted in a 57% success rate.

The cases involving $\sigma = 4$ ft/s or $(\delta_e)_{\max} = 0.10$ rad must be viewed as the extreme cases. This level of turbulence intensity is that associated with flying in severe turbulence, where controlling the aircraft becomes very difficult. Understandably, under such conditions, detection of airframe icing through the aircraft flying qualities would be far from practical. Likewise, elevator amplitudes of 0.10 rad (±5.7 deg) would subject the passengers and the airframe to unacceptable periodic load factors. Nonetheless, these cases are also shown in Table 6 to establish clear boundaries for the validity of the proposed method.

Conclusions

A method relying on ANNs and SOMs was developed to detect the presence of airframe ice from the dynamic response of an aircraft to known elevator inputs. A linear model of the longitudinal dynamics of the de Havilland DHC-6 with and without tail ice was employed to validate the method. Aircraft stability and control derivatives were modified to account for artificial tail ice and its effects on response to elevator inputs. The major thrust of this research was placed on identification of the effects of artificial tail ice on the longitudinal aircraft dynamics because of the availability of flight-test data.

It was shown that the effects of atmospheric turbulence could be differentiated from the effects of ice given sufficiently large elevator inputs. ANN models of the system state variables were developed using a backpropagation algorithm and were shown to be in good agreement with the flight-test data. Therefore, it was concluded that the ANNs effectively learned the aircraft dynamics for the purpose of this research. These ANN models were compared to each other

to determine if models representing an iced aircraft could be differentiated from those representing a clean aircraft.

A one-dimensional Kohonen SOM was created and used to distinguish an iced configuration from a clean one automatically. In calm air, the method was shown to work perfectly, requiring very small control inputs. However, as the turbulence intensity was increased, the magnitude of the required control input increased as well. With reasonable levels of turbulence encountered in most operational environments, the method was shown to accurately identify airframe icing approximately 75% of the time. This level of identification was achieved with reasonably small elevator deflections and without subjecting the passengers and the airframe to undue load factors.

Appendix: Elements of State and Control Matrices

The elements of the state matrix $[A]$ are

$$A_{1,1} = \frac{1}{2\mu}\left[2C_{L_1}\tan(\Theta_1) + C_{x_u}\right], \qquad A_{1,2} = \frac{C_{x_\alpha}}{2\mu},$$

$$A_{1,3} = -\frac{C_{L_1}}{2\mu}, \qquad A_{1,4} = 0, \qquad A_{2,1} = \frac{\left(2C_{L_1} - C_{z_u}\right)}{-2\mu + C_{z_{\dot\alpha}}}$$

$$A_{2,2} = \frac{-C_{z_\alpha}}{-2\mu + C_{z_{\dot\alpha}}}, \qquad A_{2,3} = \frac{C_{L_1}\tan(\Theta_1)}{-2\mu + C_{z_{\dot\alpha}}}$$

$$A_{2,4} = \frac{-\left(2\mu + C_{z_q}\right)}{-2\mu + C_{z_{\dot\alpha}}}, \qquad A_{3,1} = A_{3,2} = A_{3,3} = 0$$

$$A_{3,4} = 1, \qquad A_{4,1} = \frac{-C_{m_{\dot\alpha}}C_{z_u} + C_{m_u}\left(-2\mu + C_{z_{\dot\alpha}}\right) + 2C_{m_{\dot\alpha}}C_{L_1}}{\left(-2\mu + C_{z_{\dot\alpha}}\right)i_{yy}}$$

$$A_{4,2} = \frac{C_{m_\alpha}\left(-2\mu + C_{z_{\dot\alpha}}\right) - C_{m_{\dot\alpha}}C_{z_\alpha}}{\left(-2\mu + C_{z_{\dot\alpha}}\right)i_{yy}}$$

$$A_{4,3} = \frac{C_{m_{\dot\alpha}}C_{L_1}\tan(\Theta_1)}{\left(-2\mu + C_{z_{\dot\alpha}}\right)i_{yy}}$$

$$A_{4,4} = \frac{C_{m_{\dot\alpha}}\left(-2\mu - C_{z_q}\right) + C_{m_q}\left(-2\mu + C_{z_{\dot\alpha}}\right)}{\left(-2\mu + C_{z_{\dot\alpha}}\right)i_{yy}}$$

The elements of control matrix $[B]$ are

$$B_{1,1} = B_{1,2} = B_{1,3} = B_{1,4} = 0, \qquad B_{2,1} = B_{2,2} = B_{2,3} = 0$$

$$B_{2,4} = \frac{-\left(C_{z_{\delta e}}\right)}{-2\mu + C_{z_{\dot\alpha}}}, \qquad B_{3,1} = B_{3,2} = B_{3,3} = B_{3,4} = 0$$

$$B_{4,1} = B_{4,2} = B_{4,3} = 0$$

$$B_{4,4} = \frac{-C_{m_{\dot\alpha}}C_{z_{\delta e}} + C_{m_{\delta e}}\left(-2\mu + C_{z_{\dot\alpha}}\right)}{\left(-2\mu + C_{z_{\dot\alpha}}\right)i_{yy}}$$

Acknowledgment

The authors would like to express their gratitude to Thomas P. Ratvasky from NASA John H. Glenn Research Center at Lewis Field for providing the flight-test data for this research.

References

[1]Bragg, M. B., Gregorek, G. M., and Lee, J. D., "Experimental and Analytical Investigation into Airfoil Icing," *Proceedings of 14th Congress of the International Council of the Aeronautical Sciences*, Vol. 2, Association Aeronautique et Astronautique de France, Paris, 1984, pp. 1127–1138.

[2]Bragg, M. B., Gregorek, G. M., and Lee, J. D., "Airfoil Aerodynamics in Icing Conditions," *Journal of Aircraft*, Vol. 23, No. 1, 1986, pp. 76–81.

[3]Shaw, R. J., Potapczuk, M. G., and Bidwell, C. S., "Predictions of Airfoil Aerodynamic Performance Degradation Due to Icing," *Fourth Symposium on Numerical and Physical Aspects of Aerodynamic Flows*, California State Univ., Long Beach, CA, Jan. 1989.

[4]Shin, J., and Bond, T. H., "Experimental and Computational Ice Shapes and Resulting Drag Increases for a NACA 0012 Airfoil," NASA CR-193000, Jan. 1992.

[5]Papadakis, M., Alansata, S., and Seltmann, M., "Experimental Study of Simulated Ice Shapes on a NACA-0011 Airfoil," AIAA Paper 99-0096, Jan. 1999.

[6]Bragg, M. B., and Lee, S., "Effects of Simulated-Spanwise Ice Shapes on Airfoils: Experimental Investigation," AIAA Paper 99-0092, Jan. 1999.

[7]Ratvasky, T. P., and van Zante, J. F., "In-Flight Aerodynamic Measurements of an Iced Horizontal Tailplane," AIAA Paper 99-0638, Jan. 1999.

[8]van Zante, J. F., and Ratvasky, T. P., "Investigation of Dynamic Flight Maneuvers with an Iced Tailplane," AIAA Paper 99-0371, Jan. 1999.

[9]Ranaudo, R. J., Mikkelson, K. L., McKnight, R. C., Ide, R. F., Reehorst, A. L., Jordan, J. L., Schinstock, W. C., and Platz, S. J., "The Measurement of Aircraft Performance and Stability and Control After Flight Through Natural Icing Conditions," NASA TM-87265, April 1986.

[10]Ranaudo, R. J., Reehorst, A. L., Bond, T. H., and O'Mara, T. M., "Determination of Longitudinal Aerodynamic Derivatives Using Flight Data from an Icing Research Aircraft," NASA TM-101427, 1989; also AIAA Paper 89-0754, Jan. 1989.

[11]Batterson, J. G., and O'Mara, T. M., "Estimation of Longitudinal Stability and Control Derivatives for an Icing Research Aircraft from Flight Data," NASA TM-4099, March 1989.

[12]Ratvasky, T. P., and Ranaudo, R. J., "Icing Effects on Aircraft Stability and Control Determined from Flight Data—Preliminary Results," NASA TM-105977, 1993; also AIAA Paper 93-0398, Jan. 1993.

[13]Hess, R. A., "Use of Back Propagation with Feedforward Neural Networks for the Aerodynamic Estimation Problem," *Proceedings of AIAA Atmospheric Flight Mechanics Conference*, AIAA, Washington, DC, 1993, pp. 233–245; also AIAA Paper 93-3638, 1993.

[14]Ghosh, A. K., Raisinghani, S. C., and Khubchandani, S., "Estimation of Aircraft Lateral–Directional Parameters Using Neural Networks," *Journal of Aircraft*, Vol. 35, No. 6, 1998, pp. 876–881.

[15]McMillen, R. L., Steck, J. E., and Rokhsaz, K., "Application of an Artificial Neural Network as a Flight-Test Data Estimator," *Journal of Aircraft*, Vol. 32, No. 5, 1995, pp. 1088–1094.

[16]Etkin, B., *Dynamics of Flight—Stability and Control*, 2nd ed., Wiley, New York, 1982, pp. 13–45, 128–148.

[17]Roskam, J., *Airplane Flight Dynamics and Automatic Flight Controls, Part I*, Roskam Aviation and Engineering Corp., Ottawa, KS, 1979.

[18]Johnson, M. D., "Using Artificial Neural Networks and Self-Organizing Maps for Detection of Airframe Icing," M.S. Thesis, Dept. of Aerospace Engineering, Wichita State Univ., Wichita, KS, May 2000.

[19]Narendra, K. S., and Parthasarathy, K., "Identification and Control of Dynamical Systems Using Neural Networks," *IEEE Transactions on Neural Networks*, Vol. 1, No. 1, 1990, pp 4–27.

[20]Rumelhart, D. E., Smolensky, P., McClelland, J. L., Hinton, G. E., "Schemata and Sequential Thought Processes in PDP Models," *Parallel Distributed Processing—Explorations in the Microstructure of Cognition, Volume 2: Psychological and Biological Models*, edited by J. L. McClelland and D. E. Rumelhart, MIT Press, Cambridge, MA, 1986, pp. 7–57.

[21]Smolensky, P., "Neural and Conceptual Interpretation of PDP Models," *Parallel Distributed Processing—Explorations in the Microstructure of Cognition, Voume 2: Psychological and Biological Models*, edited by J. L. McClelland and D. E. Rumelhart, MIT Press, Cambridge, MA, 1986, pp. 390–431.

[22]Rumelhart, D. E., Hinton, G. E., and Williams, R. J., "Learning Internal Representations by Error Propagation," *Parallel Distributed Processing—Explorations in the Microstructure of Cognition, Voume 1: Foundations,* edited by J. L. McClelland and D. E. Rumelhart, MIT Press, Cambridge, MA, 1986, pp. 318–362.

[23]Fausett, L., *Fundamentals of Neural Networks*, Prentice–Hall, Englewood Cliffs, NJ, 1994, pp. 169–187.

[24]Hoblit, F. M., *Gust Loads on Aircraft: Concepts and Applications*, AIAA Education Series, AIAA, Washington, DC, 1988, pp. 42–51.

[25]Hancock, G. J., *An Introduction to the Flight Dynamics of Rigid Aeroplanes*, Ellis Horwood, New York, 1995, pp. 231–235.